Proceedings of CONF-MSS 2025 Symposium: Automation and Smart Technologies in Petroleum Engineering
DOI: 10.54254/2755-2721/149/2025.KL22381

Research Progress on Metal-Based Materials in Photocatalytic CO_2 Reduction

Jiaxin Song

East China University of Science and Technology, Shanghai, China
23013885@mail.ecust.edu.cn

Abstract: The photocatalytic reduction of CO_2 into value-added chemicals is regarded as a vital approach to alleviate the environmental and energy crises. Photocatalytic technology is more energy-efficient and environmentally friendly compared to electrochemical, thermochemical, and other technologies, offering broad application prospects. Therefore, it is crucial to select high-performance photocatalytic materials. Metal compounds stand out in the field of photocatalysis due to their tunable band structures abundant active sites and excellent chemical stability. This review systematically summarizes the latest progress of metal-based materials, including metal oxides such as TiO_2, CuO, Cu_2O, WO_3, as well as metal sulfides, metal phosphides, and metal-organic frameworks (MOFs), focusing on the mechanisms of strategies such as crystal engineering, heterojunction construction, and defect engineering in enhancing photocatalytic performance. Finally, it discusses the prospects and challenges of photocatalytic CO_2 reduction technology, aiming to provide theoretical references for the development of ideal and efficient photocatalytic systems, contributing to the achievement of carbon neutrality goals.

Keywords: photocatalytic, CO_2, carbon neutrality

1. Introduction

The year 2024 was the hottest year on record [1], with global average temperatures rising by approximately 1.55°C compared to pre-industrial levels [2]. This increase is closely related to the emission of greenhouse gases: in 2022, the atmospheric CO_2 concentration surged from 278 ppm in pre-industrial times to 420 ppm [3]. The extreme weather events, such as glacier melting and droughts, triggered by global warming pose a severe threat to ecological security. Therefore, CO_2 capture and utilization technologies (CCU) are urgently needed to address environmental and energy crises [4,5].

Among various technologies, photocatalysis has emerged as a promising candidate due to its solar-driven nature and characteristics of ambient temperature and pressure reactions, offering advantages such as low energy consumption, environmental friendliness, and sustainability [6,7]. In recent years, significant progress has been made in photocatalytic research. For example, Liu et al. developed P-g-C_3N_4 nanotubes that achieved a 13.92-fold increase in CH_4 yield compared to traditional g-C_3N_4 through optimized band structure [8]. Abdullah et al. constructed a 2D/2D ZnV_2O_6 -pCN heterojunction system. The modified surface charge enhanced the CH_3OH yield up to 3742 μmol $gcat^{-1}$, which is 1.15 and 5 times higher than that of pure ZnV_2O_6 and pCN, respectively [9].

However, photocatalytic reduction of CO_2 technology still faces many challenges, such as low light utilization efficiency [10,11], anatase TiO_2, for example, is only active under ultraviolet (UV)

DOI: 10.54254/2755-2721/149/2025.KL22381

light, and the visible light response of g-C_3N_4 is limited to below 460 nm [12]. Additionally, high carrier recombination rates, competition with hydrogen evolution reactions, poor long-term stability, and low product selectivity severely limit the practical application of photocatalytic technology [13].

Metal compounds, with their tunable band structures, abundant active sites, and good chemical stability, hold great potential [14]. Based on this, this review summarizes the research progress of metal-based photocatalytic materials and elaborates on optimization strategies such as defect engineering, crystal facet control, and heterojunction construction, aiming to provide a theoretical framework for building efficient, stable, and selective photocatalytic systems and to promote the resource utilization of CO_2.

2. TiO_2-Based Photocatalytic Materials

Since Inoue et al. pioneered photocatalytic CO_2 reduction in 1979 [15], a variety of photocatalytic materials have been extensively studied. As the earliest discovered and widely used photocatalytic material, TiO_2 has become one of the most promising photocatalysts due to its excellent photostability, environmental friendliness, and low cost [16]. However, its photocatalytic CO_2 reduction performance is still limited by several factors: (1) insufficient surface active sites for CO_2 adsorption and weak CO_2 activation ability; (2) high carrier recombination rate and low utilization efficiency; (3) a wide bandgap of ~3.2 eV that only responds to UV light, with visible light utilization less than 5% [17,18]. To address these bottlenecks, researchers have developed various modification strategies.

2.1. Crystal Engineering

Crystal engineering primarily involves improving catalytic performance by altering the crystal structure of TiO_2, including elemental doping, morphology control, and crystal facet control. This section mainly discusses elemental doping and morphology control.

Elemental doping can effectively adjust the band structure, enhancing light absorption and carrier utilization efficiency [19]. Asahi et al. first demonstrated that nitrogen doping could shift the valence band upward and reduce the bandgap, extending light response to the visible region [20]. Anna et al. achieved co-doping of Mo/W metal elements, forming functional groups such as hydroxyl radicals on the TiO_2 surface, which significantly improved carrier separation efficiency through synergistic effects [21].

Morphological regulation, by altering parameters such as surface area, crystallinity, and porosity, affects processes like CO_2 activation and adsorption, charge separation, and intermediate desorption [22,23]. Patricia Reñones et al. prepared mesoporous TiO_2 1-D nanofibers via electrospinning-sol-gel method, which exhibited better nanocrystalline connectivity than traditional TiO_2, promoting rapid charge transport and higher selectivity for CH_4 and CH_3OH [24].

2.2. Heterojunction Construction

Combining TiO_2 with other semiconductors to form heterojunction catalysts (n-n heterojunctions, p-n heterojunctions, Z-scheme heterojunctions, etc.) can significantly enhance carrier separation and optimize photocatalytic performance. Ali's team developed an HCNS@TiO_2 heterojunction catalyst that promoted rapid electron transfer at the interface between HCNS and TiO_2, increasing CH_3OH yield to 11.3 μmol $gcat^{-1}h^{-1}$, which is 10 times and over 5 times higher than that of traditional TiO_2 and g-C_4N_3 [25]. Chen et al. manufactured a $ZnIn_2S_4$ nanosheet/TiO_2 nanofiber heterojunction via electrospinning-hydrothermal process, with a maximum light absorption edge reaching 550 nm [26].

DOI: 10.54254/2755-2721/149/2025.KL22381

2.3. Active Site Design

Creating oxygen vacancies (OVs) to improve surface active sites, adjust electronic structure and bandgap, and expand light response and carrier utilization efficiency is a promising approach [27]. Studies have confirmed that surface oxygen vacancies can enhance CO_2 adsorption by binding to CO_2 oxygen atoms and bending the linear CO_2 molecule, reducing the reaction barrier for C-O bond cleavage [28]. Huang's team developed a $TiO_{2-\alpha}/WO_{3-\delta}$ heterojunction catalyst that induced local electron enrichment by regulating OVs concentration, strengthening the built-in electric field and effectively suppressing carrier recombination, resulting in a CH_4 yield of 28.11μmol $g^{-1}h^{-1}$, which is 18.6 times higher than that of traditional samples [29]. Li et al. combined interstitial carbon doping with oxygen vacancies to prepare TiO2 nanofiber membranes, altering reaction sites to accumulate CO* intermediates at Ti termini rather than desorbing them, enabling continuous hydrogenation to form methane with a yield of 55.17 μmol $g^{-1}h^{-1}$ and a selectivity of 98.3% [30].

Constructing surface frustrated Lewis pairs (FLPs) is an innovative strategy. FLPs, with spatially separated Lewis acid and Lewis base active sites, can induce CO_2 polarization and promote its heterolysis by activating both oxygen and carbon atoms in the CO_2 molecule, thereby enhancing CO_2 activation efficiency. Zhao et al. manufactured a core-shell c-TiO_2@a-$TiO_{2-x}(OH)_y$ heterostructure via disorder engineering. The mechanism of action of SFLPs is shown in Fig.1a-e,Ti(III) forms SFLPs (Fig.1i-k) with oxygen vacancies (Fig.1g,h) on the TiO_2 surface, creating high-activity sites for CO_2 reaction through protonated hydroxyl groups formed by hydrogen cleavage. The core-shell structure(Fig.1f) enhances light absorption(Fig.1l). Analysis of charge carrier mobility and the localization of energy states via inverse participation ratio (IPR) revealed that a-$TiO_{2-x}(OH)_y$ has a high concentration of self-trapped polarons and excitons (Fig.1m,n), effectively promoting carrier separation and extending carrier lifetime (Fig.1p). Fig.1o is a schematic diagram of electron migration. This material achieved a CO yield of 5.3 mmol $gcat^{-1}$ h^{-1}, which is 350 times higher than that of c-TiO_2 crystals [31].

DOI: 10.54254/2755-2721/149/2025.KL22381

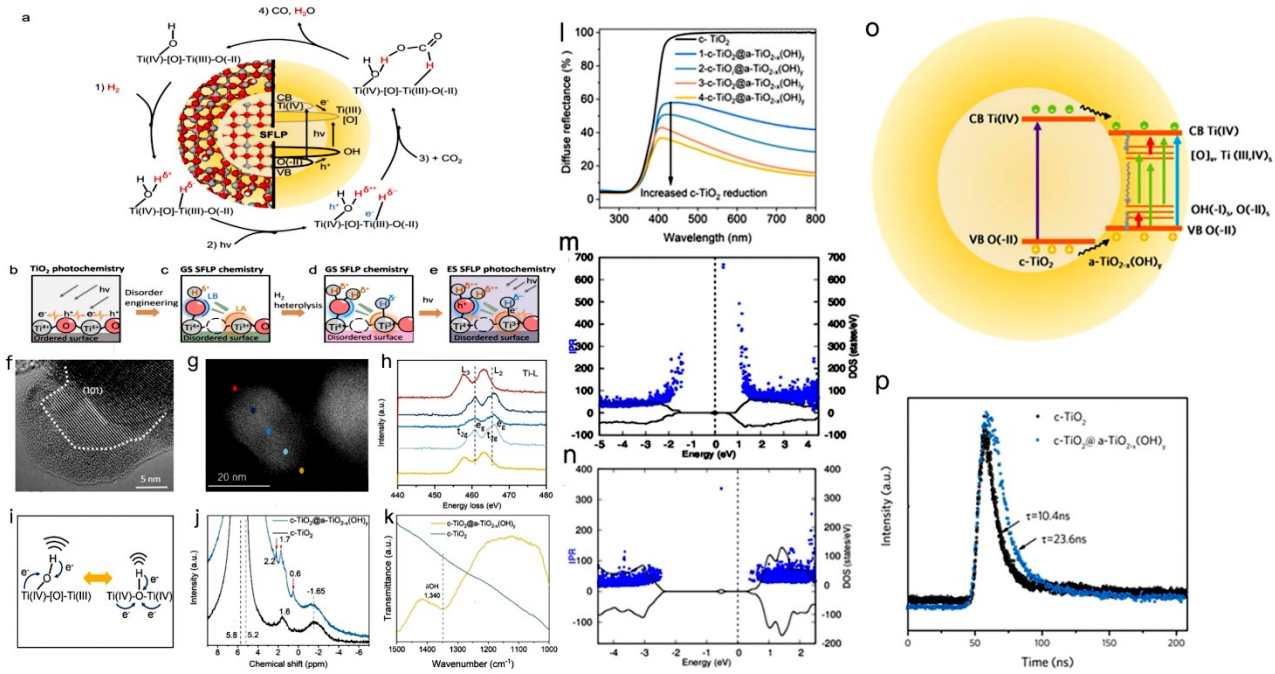

Figure 1: (a) SFLPs act on the surface of the c-TiO_2@a-$TiO_{2-x}(OH)_y$ heterostructure. (b) an unmodified crystalline surface, (c) formation of an SFLP site, (d) a ground-state SFLP site following activation by hydrogen (e) the enhanced activity excited-state SFLP generated by photoexcitation of the ground-state SFLP. (f) HR-TEM micrograph of c-TiO_2@a-$TiO_{2-x}(OH)_y$ (anatase phase). The amorphous/crystalline interfaces are marked with dotted lines. (g) High-angle annular dark-field scanning transmission electron microscopy (HAADF-STEM) image of c-TiO_2@a-$TiO_{2-x}(OH)_y$. (h) Ti-L edge EELS spectra at different positions. (i) Comparison of geometrical and electronic structures between bridging and terminal hydroxyl. j, k HMAS-NMR (j) and ATR-FTIR (k) spectra of c-TiO_2@a-$TiO_{2-x}(OH)_y$ and c-TiO_2. (l) UV–Vis-NIR diffuse reflectance spectra (DRS). m, n The total density of states (black line, right axis) and the corresponding values of the inverse participation ratio (IPR) (blue dots, left axis) for a-$TiO_{2-x}(OH)_y$ (m) and crystalline TiO_{2-x} (n) surfaces. (o) Schematic of charge carrier separation and transfer pathways in c-TiO_2@a-$TiO_{2-x}(OH)_y$. The colors of arrows indicate the wavelength of incident light. (p) Time-resolved photoluminescence spectroscopy decay curves of c-TiO_2 and c-TiO_2@a-$TiO_{2-x}(OH)_y$.

2.4. Others

In addition to the aforementioned strategies, other approaches include the use of cocatalysts, surface plasmon resonance (SPR), construction of internal electric fields, and multi-dimensional synergistic strategies. Zhang et al. decorated TiO_2 nanotubes (NTs) with carbon quantum dots (CQDs), achieving a methane yield 2.5 times higher than that of traditional TiO_2[32]. Liu et al. synthesized 2.5 wt% Ag/TiO_2 composite materials, with a methanol production rate of 135.1μmol $g^{-1}h^{-1}$ which is 9.4 times higher than that of pure TiO_2[33]. Xing et al. fluorinated single-crystal TiO_{2-x} to construct an internal electric field, enhancing carrier separation and migration efficiency and increasing methane yield tenfold to 0.98 mmol $g^{-1}h^{-1}$ compared to traditional TiO_2[34].

3. Copper-based Photocatalytic Materials

In photocatalytic reactions, the reduction ability of a semiconductor is primarily determined by the positions of its conduction band (CB) and valence band (VB).Copper-based semiconductors (such as

DOI: 10.54254/2755-2721/149/2025.KL22381

CuO, Cu_2O, and Cu_2S), with their relatively narrow band gaps (approximately 1.7 eV, 2.2 eV, and 1.2 eV respectively), and favorable conduction band (CB) states, exhibit good visible-light response and thus show significant potential in the field of photocatalysis. However, copper-based materials also exhibit several drawbacks. For instance, Cu_2O is prone to high carrier recombination rates, limited charge migration, and photo-corrosion in liquid phases, resulting in poor long-term stability [35]. To address these issues, researchers have developed various strategies.

Zhang et al. modified Cu_2O with Pd to synthesize 100Cu_2O-0.1Pd, which facilitated the transfer of photogenerated holes from Cu_2O to Pd. This modification enhanced charge migration and corrosion resistance, increasing CO yield to 0.13 μmol $g^{-1}h^{-1}$, three times higher than that of pristine Cu_2O [36]. Cui et al. prepared three-dimensional porous Cu_2O with nanoscale dendrites. The dendritic porous structure enhances the light-harvesting ability and electron transfer efficiency, resulting in a CO production rate that is 24 times higher than that of traditional Cu_2O [37]. Khatri et al. fabricated reduced graphene oxide–CuO (rGO–CuO) nanocomposites. The close energy levels of the LUMO (lowest unoccupied molecular orbital) between CuO and graphene facilitates electron transfer, overcoming the high carrier recombination rate in traditional CuO. This leads to a CH3OH production rate of 1228 μmol$g^{-1}h^{-1}$, which is seven times higher than that of pure CuO nanorods [38]. Wang et al. synthesized Cu_2O@ZnTPP heterojunction composites, constructing a Zn-O-Cu electron transfer pathway that enhanced electron migration rates, protected ZnTPP from photo-corrosion, and promoted multi-electron reactions on Cu_2O. This material achieved a CH_4 yield of 120.9 μmol $g^{-1}h^{-1}$, ten times higher than that of traditional Cu_2O, with 98.7% selectivity [39].

4. WO_3-Based Photocatalytic Materials

Tungsten trioxide (WO_3) is characterized by its wide light absorption spectrum (bandgap ~2.5 eV, with absorption extending up to 500 nm), high electron mobility (12 $cm^2V^{-1}s^{-1}$), long hole diffusion length, and excellent chemical stability under harsh conditions (e.g., acidic and oxidative environments). These attributes make WO_3 a highly attractive candidate for photocatalytic applications [40]. However, pure WO_3 still falls short of industrial photocatalytic efficiency requirements due to its relatively low CB edge potential (+0.5 eV) and rapid carrier recombination [41]. To enhance the catalytic efficiency of WO_3, various strategies, including defect engineering and heterojunction construction, have been employed.

Regulating the crystal morphology and microstructure of WO_3 is a direct approach to improving its performance. Shi et al. synthesized Cu_2O/WO_3-001 composite nanosheets (Fig.2a-f), whose favorable spatial structure increased the contact area with CO_2. WO_3-001 exhibited a maximum pore size peak at 0.41 nm (Fig.2g), and its CO2 adsorption isotherm showed a higher adsorption capacity (Fig.2h), indicating good porosity and microchannels that facilitate CO_2 adsorption. The possible electron-hole separation process (Fig.2i) involves photogenerated holes remaining in the VB of WO_3 while electrons in the CB of WO_3 transfer to the VB of Cu_2O, achieving effective charge separation.This Z-scheme electron transfer mode significantly enhanced photocatalytic performance. After 24 hours of irradiation, the yields of CO, O_2, and H_2 over this material reached 11.7, 5.7, and 0.7μmol, respectively (Fig.2j), although its stability was moderate (Fig.2k) [42].

DOI: 10.54254/2755-2721/149/2025.KL22381

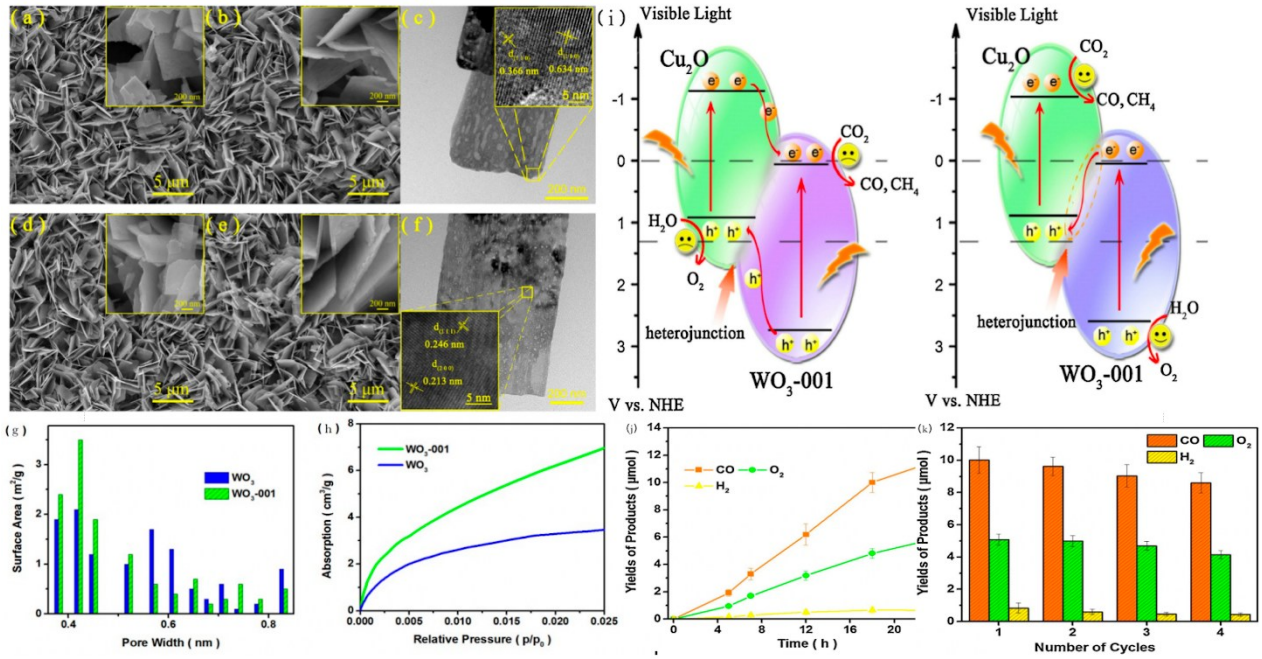

Figure 2: SEM and TEM images of WO3 (a), WO3-001 (b, c), Cu2O/WO3-001 (d) and Cu2O/WO3-001 (e, f) sample. (g) Calculated pore size distributions. (h) CO adsorptioisotherm of WO3 and WO3-001 sample. (i) Schematic illustration of the proposed charge transfer mechanisms- the common charge transfer mode and Z-scheme charge transfer mode for Cu2O/WO3-001. (j) Total yields of the products over the Cu2O/WO3-001 catalyst with different irradiation times. (k) Recyclability test of the Cu2O/WO3-001 catalyst under visible-light.

Constructing heterojunctions has shown significant effects on improving WO_3 performance.Gao et al. anchored black phosphorus quantum dots (BPQDs) onto WO_3 nanowires to form a 0D-1D direct Z-scheme heterojunction. The BPQD-WO_3 heterojunction not only achieved high CO conversion efficiency but also innovatively produced C_2H_4 [43]. Zhu et al. synthesized a 2D/1D $BiOBr_{0.5}Cl_{0.5}/WO_3$ S-scheme heterojunction, which, with the assistance of cocatalysts, achieved a CO yield of 16.68 μmol $g^{-1}h^{-1}$, nine times higher than that of traditional WO_3.Notably, the $BiOBr_{0.5}Cl_{0.5}/WO_3$ composite maintained stable photocatalytic performance over time [44].

In addition, there are various pathways such as cocatalysts and oxygen vacancy regulation.Wang et al. modified hexagonal WO_3 with Pt, which promoted local electron delocalization, increased free electron concentration, and significantly enhanced charge separation and transfer efficiency. Moreover, Pt modification improved CO_2 adsorption and activation capabilities. Within 5 hours, 0.5%Pt-WO_3 catalyzed the production of 3.64 μmol CH_4, approximately seven times higher than that of pure hexagonal WO_3[45]. Ben et al. doped C atoms into two-dimensional WO3 nanosheets and introduced oxygen vacancies, achieving a CO yield of 23.2 μmol $g^{-1}h^{-1}$ with 85.8% selectivity [46]. Zeng et al. deposited single-atom Cu and Pt on WO_3, triggering C-C coupling to photoreduce CO_2 into high-value CH_3COOH. The Cu_2Pt_2/WO_3 catalyst achieved an CH_3COOH yield of 19.41 μmol $g^{-1}h^{-1}$ with 88.1% selectivity, significantly higher than that of the original sample [47].

5. Metal-Organic Frameworks (MOFs)

In addition to semiconductor-based photocatalysts, metal-organic frameworks (MOFs) have emerged as novel and promising materials in recent years due to their excellent CO_2 adsorption capabilities and unique structural characteristics. MOFs offer several advantages: (1) high specific surface area and adjustable porous structures that enable efficient CO_2 adsorption and transformation, combined

DOI: 10.54254/2755-2721/149/2025.KL22381

with high crystallinity for superior light absorption and charge transfer capabilities;(2) modular design through diverse metal nodes and organic linkers to tailor photocatalytic performance; (3) high stability and recyclability, facilitating reuse; (4) further performance enhancement through functionalization and construction of composite systems for synergistic catalysis; (5) diverse synthesis methods, many of which are environmentally friendly [48,49]. Optimization strategies for MOFs mainly focus on modifying metal nodes and organic linkers, post-synthetic method (PSM), constructing composites with semiconductors or metal nanoparticles, and optimizing interpenetrating structures. Some recent research progress is briefly introduced below.

Lin et al. demonstrated that synthesis methods can influence surface structure and, consequently, catalytic performance. Their team developed a core-shell structured Fe/Ni-T120 material with uniform mesoporous structures (~2.5 nm) and abundant active sites, achieving a high CO yield of 9.74 mmol $g^{-1}h^{-1}$ with 92.1% selectivity [50]. The photocatalytic activity is closely related to the exposed facets. Cheng et al. investigated the photocatalytic performance of NH_2-MIL-125 (Ti) exposing high-index {112} facets. The {112} facets exhibited CO and CH_4 yields 33 and 31 times higher than those of low-index {001}/{111} facets, respectively. This was attributed to the higher affinity of {112} facets for CO_2 and the narrower HOMO-LUMO gap, which promotes charge generation and transfer [51]. Studies have shown that amino-functionalized linkers are more effective than other functional groups (such as -Br, -OH, -SH, and -NO_2) in enhancing photocatalytic efficiency [52]. Huang et al. synthesized UiO-66-NH_2 via microwave heating, which achieved a CO2 adsorption capacity of 5.8 mmol g^{-1} at 273 K and 1 bar, and a CO_2/N_2 selectivity of 66, significantly higher than the 17.8 selectivity of original UiO-66 [53].

6. Other Photocatalytic Materials

In addition to the commonly studied metal oxides, metal sulfides, phosphides, and nitrides also hold great potential.

Cheng et al. prepared a three-dimensional hierarchical $Cd_{0.8}Zn_{0.2}S$ (C8Z2S-F) with ultrathin petals. The chemical composition and element states are shown in Fig.3a and b. It features slit-like pores, a narrower bandgap width, and a more negative conduction band potential (Fig.3c-f). It exhibits an outstanding CO selectivity of 89.9% within 3 hours (Fig.3g), with CO and CH_4 yields of approximately 41.4μmol g^{-1} and 1.4μmol g^{-1}(Fig.3h,i). The mechanism of CO_2 conversion to CO and CH_4 is illustrated in Fig.3j. In CO_2-TPD measurements (Fig.3k), the strong basic adsorption peak of C8Z2S-F at 370°C has a significantly higher desorption temperature and intensity than that of C8Z2S-NP (at 320°C), indicating that C8Z2S-F has a much stronger CO_2 adsorption capacity than C8Z2S-NP. TPR (Fig.3l) shows that C8Z2S-F has a stronger photocurrent density, indicating better carrier separation and migration. The reaction mechanism is shown in Fig.3m [54].

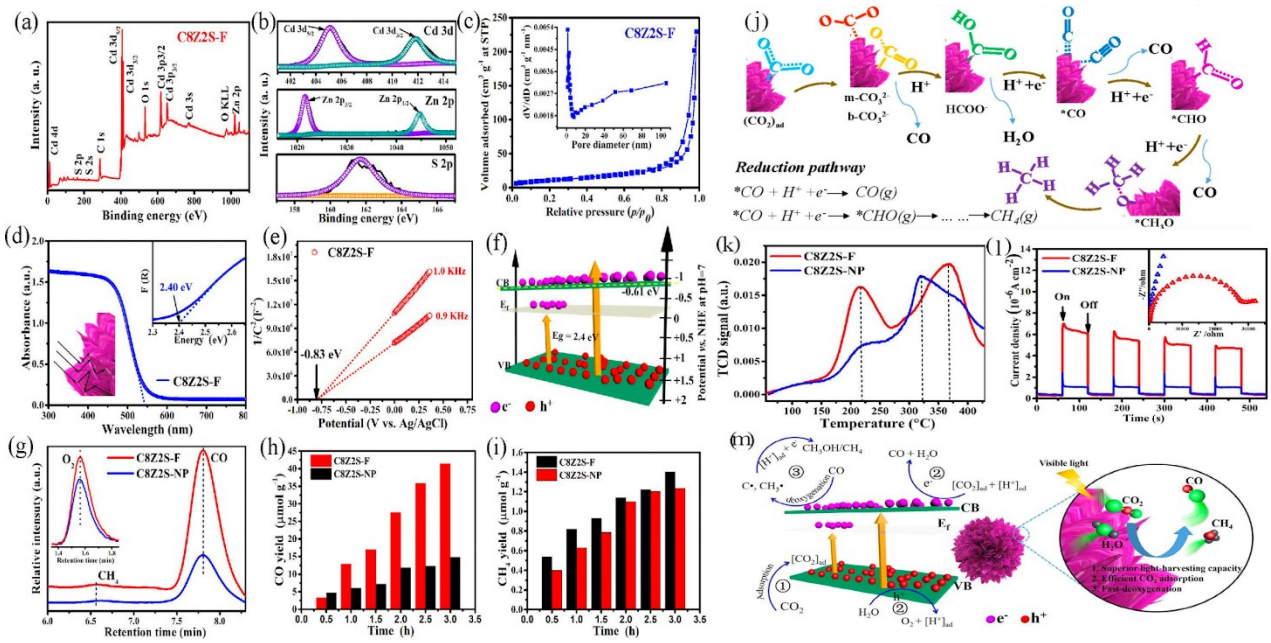

Figure 3: (a) XPS spectra. (b) High resolution XPS spectra. (c) N2 adsorption-desorption isotherms (inset indicates the pore size distribution); (d) UV-vis DRS spectra (inset shows the Kubelka-Munk function vs. photon energy curves). (e) Mott-Schottky plots. (f) Schematic of the electronic band structures of the as-obtained C8Z2S-F sample. (g) Photocatalytic products of CO2 reduction detected by original chromatograms over C8Z2S-F and C8Z2S-NP samples under visible-light irradiation for 3 h; Photocatalytic activity of CO (h) and CH4 evolution (i) over 0.03 g C8Z2S-F and C8Z2S-NP samples under visible light irradiation. Reaction conditions: deionized water (500 μL), Xe lamp(300 W). (j) Schematic of the photocatalytic reduction of CO2 by using C8Z2S-F sample as photocatalyst.CO2-TPD profiles (k) and EIS spectras (l) (inset shows the TPR curves) of C8Z2S-F and C8Z2S-NP samples.(m)Schematic of the possible photocatalytic process during the conversion of CO2 to CO and CH4.

Xu et al. synthesized metal phosphides (M-P/BP) on black phosphorus nanosheets (BP) via in situ growth, such as Co_2P/BP. The ultrafine Co_2P nanocrystals formed on the BP surface effectively adsorbed and activated CO_2 molecules through additional cobalt active sites. The Co-P charge transfer channel significantly enhanced carrier separation efficiency, achieving a CO yield of 255.1 μmol $g^{-1}h^{-1}$, nearly twice that of BP alone (141.8 μmol $g^{-1}h^{-1}$) [55]. Moreover, while semiconductor catalysts like TiO_2 typically require narrower bandgaps to respond to lower-energy infrared light, metal catalysts such as Co_2P/BP exhibit better infrared responsiveness [56].

7. Conclusions

Significant breakthroughs have been made in the field of metal-based photocatalytic CO_2 reduction in recent years. This review summarizes the research progress and performance optimization strategies of TiO_2-based, Copper-based, WO_3-based, and MOF materials, as well as their underlying mechanisms. Advances have been achieved through techniques such as atomic layer deposition and electron beam evaporation to enhance photostability, functional group modification to improve CO_2 adsorption and activation, and heterojunction construction and defect engineering to accelerate carrier migration and utilization.

In the future, metal-based photocatalytic materials for CO_2 reduction can be integrated with digital twin technology to develop dynamic intelligent catalytic systems. They can also be coupled with

DOI: 10.54254/2755-2721/149/2025.KL22381

biological systems to construct biomimetic photosynthetic systems, thereby promoting selective control of products. By incorporating photocatalytic materials into diverse industries such as construction and transportation, innovative solutions can be provided for the global carbon neutrality goal. However, there remain areas that require further exploration, as follows.

1. The carrier recombination mechanism are not yet fully understood, limiting the improvement of carrier efficiency. Advanced in situ characterization techniques, combined with density functional theory (DFT) and other theoretical calculations, are needed to elucidate interfacial charge transfer and surface reaction kinetics mechanisms.
2. The complex multiple-proton and electron coupling processes result in low selectivity for C2+ products. There is a need to reveal the structure-activity relationships of intermediate products and establish predictive models based on descriptors (e.g., d-band center) to explore photocatalysts and pathways with higher selectivity for high-value products.
3. The long-term stability and recyclability of catalysts in large-scale applications urgently need to be verified. It is necessary to develop a catalyst life prediction system in combination with machine algorithms and establish an intelligent ASTM evaluation system. The transition of laboratory achievements to industrialization should be promoted through interdisciplinary integration and technological innovation.

References

[1] *World Meteorological Organization. (2024) WMO Confirms 2024 as Warmest Year on Record at About 1.55°C Above Pre-industrial Level. Retrieved from https://wmo.int/news/media-centre/wmo-confirms-2024-warmest-year-record-about-155degc-above-pre-industrial-level*

[2] *Associated Press. (2024) Earth Breaks Yearly Heat Record and Lurches Past Dangerous Warming Threshold. AP News.Retrieved from https://apnews.com/article/climate-change-warming-hot-record-2024-disasters-12f899f071fcdbd051ad49a872611e92*

[3] *National Aeronautics and Space Administration. (2024) Temperatures Rising: NASA Confirms 2024 Warmest Year on Record. Retrieved from https://www.nasa.gov/news-release/temperatures-rising-nasa-confirms-2024-warmest-year-on-record/*

[4] *Mac Dowell, N., Fennell, P., Shah, N., et al. (2017) The Role of CO2 Capture and Utilization in Mitigating Climate Change. Nature Clim Change, 7, 243–249. https://doi.org/10.1038/nclimate3231*

[5] *Hepburn, C., Adlen, E., Beddington, J., et al. (2019) The Technological and Economic Prospects for CO2 Utilization and Removal. Nature, 575, 87–97. https://doi.org/10.1038/s41586-019-1681-6*

[6] *Saravanan, A., et al. (2021) A Comprehensive Review on Different Approaches for CO2 Utilization and Conversion Pathways. Chemical Engineering Science, 236, 116515.*

[7] *Li, D., et al. (2024) Strategies for Optimizing the Efficiency and Selectivity of Photocatalytic Aqueous CO2 Reduction: Catalyst Design and Operating Conditions. Nano Energy, 110460.*

[8] *Liu, B., et al. (2017) Phosphorus-Doped Graphitic Carbon Nitride Nanotubes with Amino-Rich Surface for Efficient CO2 Capture, Enhanced Photocatalytic Activity and Product Selectivity. ACS Appl Mater Interfaces. DOI: 10.1021/acsami.7b17503*

[9] *Bafaqeer, A., Tahir, M., and Amin, N.A.S. (2019) Well-Designed ZnV2O6/g-C3N4 2D/2D Nanosheets Heterojunction with Faster Charges Separation via pCN as Mediator Towards Enhanced Photocatalytic Reduction of CO2 to Fuels. Applied Catalysis B: Environmental, 242, 312–326.*

[10] *Zhao, L., et al. (2023) Efficient Photoreduction of Carbon Dioxide into Carbon-Based Fuels: A Review. Environmental Chemistry Letters, 21, 1499–1513.*

[11] *Gao, Y., et al. (2020) Recent Advances in Visible-Light-Driven Conversion of CO2 by Photocatalysts into Fuels or Value-Added Chemicals. Carbon Resources Conversion, 3, 46–59.*

[12] *Zhao, S., et al. (2012) g-C3N4/TiO2 Hybrid Photocatalyst with Wide Absorption Wavelength Range and Effective Photogenerated Charge Separation. Separation and Purification Technology, 99, 50–54.*

[13] *Gong, et al. (2016) CO2 Photo-Reduction: Insights into CO2 Activation and Reaction on Surfaces of Photocatalysts. Energy & Environmental Science.*

[14] *Tachibana, Y., Vayssieres, L., and Durrant, J.R. (2012) Artificial Photosynthesis for Solar Water-Splitting. Nature Photonics, 6, 511–518.*

[15] Noue, T., Fujishima, A., Konishi, S., et al. (1979) Photoelectrocatalytic Reduction of Carbon Dioxide in Aqueous Suspensions of Semiconductor Powders. Nature, 277, 637–638. https://doi.org/10.1038/277637a0

[16] Yuan, Z., et al. Enhancing Photocatalytic CO2 Reduction with TiO2-Based Materials: Strategies, Mechanisms, Challenges, and Perspectives. Environmental Science and Ecotechnology, 20, 100368.

[17] Wang, S., et al. (2021) Mechanistic Insight into Photocatalytic CO2 Reduction by a Z-Scheme gC3N4/TiO2 Heterostructure. New Journal of Chemistry, 45, 11474–11480.

[18] Zhou, Y., et al. (2022) Photocatalytic Reduction of CO2 into CH4 over Ru-Doped TiO2: Synergy of Ru and Oxygen Vacancies. Journal of Colloid and Interface Science, 608, 2809–2819.

[19] Kmentová, H., et al. (2025) Tuning CO2 Reduction Selectivity via Structural Doping of TiO2 Photocatalysts. Journal of CO2 Utilization, 91, 103008.

[20] Asahi, R., et al. (2001) Visible-Light Photocatalysis in Nitrogen-Doped Titanium Oxides. Science, 293, 269–271.

[21] Khlyustova, A., et al. (2020) Doped TiO2: The Effect of Doping Elements on Photocatalytic Activity. Materials Advances, 1.

[22] Di, T., Zhang, J., Cheng, B., et al. (2018) Hierarchically Nanostructured Porous TiO2(B) with Superior Photocata lytic CO2 Reduction Activity. Science China Chemistry, 61, 344–350. https://doi.org/10.1007/s11426-017-9174-9

[23] Bai, S., Wang, L., Li, Z. and Xiong Y.Z. (2017) Facet-Engineered Surface and Interface Design of Photocatalytic Materials. Advanced Science. Advanced Science, 4(1), 1600216.

[24] Reñones, P., et al. (2016) Hierarchical TiO2 Nanofibres as Photocatalyst for CO2 Reduction: Influence of Morphology and Phase Composition on Catalytic Activity. Journal of CO2 Utilization, 15, 24–31.

[25] Dehkordi, A.B., et al. (2020) Preparation of Hierarchical g-C3N4@TiO2 Hollow Spheres for Enhanced Visible-Light Induced Catalytic CO2 Reduction. Solar Energy, 205, 465–473.

[26] Chen, S., et al. (2018) In-Situ Growth of ZnIn2S4 Decorated on Electrospun TiO2 Nanofibers with Enhanced Visible-Light Photocatalytic Activity. Chemical Physics Letters, 706, 68–75.

[27] Wang, J., et al. (2022) A Review on TiO2−x-Based Materials for Photocatalytic CO2 Reduction. Nanoscale, 14, 11512–11528.

[28] Zhang, W., et al. (2021) Black Single-Crystal TiO2 Nanosheet Array Films with Oxygen Vacancy on {001} Facets for Boosting Photocatalytic CO2 Reduction. Journal of Alloys and Compounds, 870, 159400.

[29] Huang, S., Wang, J.S., Bao, R., Yi, J.H., Liu, L., Kong, X.(2024) Oxygen Vacancy-Induced Modulation of the Built-in Electric Field of TiO2-α/WO3-δ for Enhanced CO2 Photoreduction. Ceramics International, 50, 38323–38330. https://doi.org/10.1016/j.ceramint.2024.07.196

[30] Li, Y., Ren, Z., and Gu, M. (2022) Synergistic Effect of Interstitial C Doping and Oxygen Vacancies on the Photoreactivity of TiO2 Nanofibers Towards CO2 Reduction. Applied Catalysis B: Environmental.

[31] Li, Z., et al. (2022) Engineered Disorder in CO2 Photocatalysis. Nature Communications, 13, 7205.

[32] Zhang, J., Xu, J., and Tao, F. (2021) Interface Modification of TiO2 Nanotubes by Biomass-Derived Carbon Quantum Dots for Enhanced Photocatalytic Reduction of CO2. ACS Applied Energy Materials, 4, 13120–13131.

[33] Liu, E., et al. (2014) Photocatalytic Reduction of CO2 into Methanol over Ag/TiO2 Nanocomposites Enhanced by Surface Plasmon Resonance. Plasmonics, 9, 61–70.

[34] Xing, M., et al. (2018) Modulation of the Reduction Potential of TiO2-x by Fluorination for Efficient and Selective CH4 Generation from CO2 Photoreduction. Nano Letters. DOI: 10.1021/acs.nanolett.8b00197

[35] Li, J.Y., et al. (2019) One-Dimensional Copper-Based Heterostructures Toward Photo-Driven Reduction of CO2 to Sustainable Fuels and Feedstocks. Journal of Materials Chemistry A, 7, 8676–8689.

[36] Zhang, X., et al. (2021) Palladium-Modified Cuprous(I) Oxide with {100} Facets for Photocatalytic CO2 Reduction. Nanoscale, 13.

[37] Xue, J., et al. (2022) Three-Dimensional Porous Cu2O with Dendrite for Efficient Photocatalytic Reduction of CO2 Under Visible Light. Applied Surface Science, 581.

[38] Gusain, R., et al. (2016) Reduced Graphene Oxide-CuO Nanocomposites for Photocatalytic Conversion of CO2 into Methanol Under Visible Light Irradiation. Applied Catalysis B: Environmental, 352–362.

[39] Wang, Z., et al. (2024) Constructing Cuprous Oxide-Modified Zinc Tetraphenylporphyrin Ultrathin Nanosheets Heterojunction for Enhanced Photocatalytic Carbon Dioxide Reduction to Methane. Journal of Colloid and Interface Science, 667, 212–222.

[40] Huang, G., et al. (2022) Unique Insights into Photocatalytic VOCs Oxidation Over WO3/Carbon Dots Nanohybrids Assisted by Water Activation and Electron Transfer at Interfaces. Journal of Hazardous Materials, 423, 127134.

[41] Liu, Z., Wu, J., and Zhang, J. (2016) Quantum Dots and Plasmonic Ag Decorated WO3 Nanorod Photoanodes with Enhanced Photoelectrochemical Performances. International Journal of Hydrogen Energy, 41, 20529–20535.

[42] Shi, W., et al. (2019) Controllable Synthesis of Cu2O Decorated WO3 Nanosheets with Dominant (001) Facets for Photocatalytic CO2 Reduction Under Visible-Light Irradiation. Applied Catalysis B: Environmental, 243, 236–242.

[43] Gao, W., et al. (2020) Anchoring of Black Phosphorus Quantum Dots onto WO3 Nanowires to Boost Photocatalytic CO2 Conversion into Solar Fuels. Chemical Communications, 56, 7777–7780.

[44] Zhu, B., et al. (2022) Enhanced Photocatalytic CO2 Reduction Over 2D/1D BiOBr0.5Cl0.5/WO3 S-Scheme Heterostructure. Acta Physico-Chimica Sinica, 38, 2111008.

[45] Wang, H., et al. (2020) Photocatalytic CO2 Reduction Over Platinum Modified Hexagonal Tungsten Oxide: Effects of Platinum on Forward and Back Reactions. Applied Catalysis B: Environmental, 263.

[46] Lei, B., et al. (2022) C-Doped Induced Oxygen-Vacancy in WO3 Nanosheets for CO2 Activation and Photoreduction. ACS Catalysis, 12, 9670–9678.

[47] Zeng, D., et al. (2023) Photocatalytic Conversion of CO2 to Acetic Acid by CuPt/WO3: Chloride Enhanced CC Coupling Mechanism. Applied Catalysis B: Environmental, 323, 122177.

[48] Chen, Y., et al. (2017) Metal–Organic Frameworks (MOFs) for Photocatalytic CO2 Reduction. Catalysis Science & Technology, 7, 4893–4904.

[49] Liu, Y., et al. (2024) Recent Advances in Amino-Functionalized Metal–Organic Frameworks for Sustainable Photocatalytic Carbon Dioxide Reduction. Separation and Purification Technology, 131023.

[50] Gu, L., et al. (2022) Optimization of Fe/Ni Organic Frameworks with Core–Shell Structures for Efficient Visible-Light-Driven Reduction of Carbon Dioxide to Carbon Monoxide. Nanoscale, 14, 15821–15831.

[51] Cheng, X.M., Zhang, X.Y., Dao, X.Y., et al. (2022) High-Index Facets Exposed on Metal–Organic Framework for Boosting Photocatalytic Carbon Dioxide Reduction. Chemical Engineering Journal, 431, 134125.

[52] Shen, L., et al. (2015) Electronic Effects of Ligand Substitution on Metal–Organic Framework Photocatalysts: The Case Study of UiO-66. Physical Chemistry Chemical Physics, 17, 117–121.

[53] Huang, A., Wan, L., and Caro, J. (2018) Microwave-Assisted Synthesis of Well-Shaped UiO-66-NH2 with High CO2 Adsorption Capacity. Materials Research Bulletin, 98, 308–313.

[54] Cheng, L., et al. (2021) Structural Engineering of 3D Hierarchical Cd0.8Zn0.2S for Selective Photocatalytic CO2 Reduction. Chinese Journal of Catalysis, 42, 131–140.

[55] Xu, Y., et al. (2022) In-Situ Growth of Metal Phosphide-Black Phosphorus Heterojunction for Highly Selective and Efficient Photocatalytic Carbon Dioxide Conversion. Journal of Colloid and Interface Science, 616, 641–648.

[56] Zhao, L., et al. (2023) Efficient Photoreduction of Carbon Dioxide into Carbon-Based Fuels: A Review. Environmental Chemistry Letters, 21, 1499–1513.